ORIGINAL ARTICLE

Proposed graphene nanospaser

Vadym Apalkov[1] and Mark I Stockman[1,2,3]

We propose a novel nanospaser that operates in the mid-infrared region and utilizes a nanopatch of graphene as its plasmonic core and a quantum-well cascade as its gain medium. This design takes advantage of the low optical losses in graphene resulting from its high electron mobility. The proposed quantum cascade graphene spaser generates optical fields with unprecedentedly high nanolocalization, which is characteristic of graphene plasmons. This spaser will be an efficient nanosource of intense and coherent hot-spot fields in the mid-infrared spectral region with potential widespread applications in mid-infrared nanoscopy, nanospectroscopy, nanolithography, and optoelectronic information processing.

INTRODUCTION

A spaser (Surface Plasmon Amplification by Stimulated Emission of Radiation),[1–11] which is the nanoplasmonic counterpart of a laser, consists of a plasmonic nanoparticle coupled to an active (gain) medium. Spasing results in the coherent generation of surface plasmons with nanolocalized, intense, coherent optical fields. One of the limitations on the spaser is imposed by the high damping rate of the surface plasmon excitations in plasmonic metals. Here, we propose a novel nanospaser in the mid-infrared that utilizes a nanopatch of graphene as its plasmonic core and a quantum-well cascade as its gain medium. This design takes advantage of the low optical losses in graphene due to its high electron mobility.[12,13] In contrast to earlier designs of quantum cascade lasers that employed plasmonic waveguides[14,15] and subwavelength resonators,[16] the proposed quantum cascade graphene spaser generates optical fields with unprecedentedly high nanolocalization, which is characteristic of graphene plasmons.[17] This spaser will be an efficient nanosource of intense and coherent hot-spot fields in the mid-infrared spectral region with potential widespread applications in mid-infrared nanoscopy, nanospectroscopy, nanolithography and optoelectronic information processing.

Quantum nanoplasmonics has become a rapidly growing field of nanooptics due to the unique ability of plasmonic systems to strongly enhance subwavelength optical fields[18] while maintaining their quantum properties.[19] This plasmonic enhancement is the basis for many nanoplasmonic applications.[20–25] There is particular interest in mid-infrared near-field spectroscopy because of the distinct spectral signatures of important molecular, biological and condensed-matter systems, including macromolecules and graphene.[26,27] For further development of plasmonics and near-field optics and their applications, it is crucial to have a coherent source of intense local fields on the nanoscale, in particular in the mid-infrared.

Here, we propose a novel spaser as a coherent quantum generator of surface plasmons in nanostructured graphene. The plasmonic core of this spaser is a graphene-monolayer nanopatch, and its active (gain) element is a quantum-well cascade with a design similar to that of the active element of quantum cascade lasers[28] (Figure 1a).

Graphene is a layer of crystalline carbon that is only one-atom thick.[29–31] The low-energy electronic excitations of graphene are described by the chiral, relativistic massless Dirac–Weyl equation. Doped graphene is known to possess plasmonic properties with a potentially high plasmonic quality factor (low optical loss) due to its high electron mobility.[12,13,27,32–34] The size of the graphene nanopatch may be as small as $\leqslant 10$ nm. Graphene possesses unprecedented tight localization of local plasmonic fields at its surface, which provides a unique opportunity for constructing an electrically pumped mid- to near-infrared nanospaser with coherent optical fields of extremely high concentration and intensity (Figure 2). The proposed nanospaser will be the first electrically pumped nanospaser: the previous nanospasers were optically pumped,[4,11] whereas the electrically pumped spasers had mode volumes with a microscale size in at least one dimension.[5,6]

MODEL AND MAIN EQUATIONS

The chiral nature of the electronic states in graphene results in a strong suppression of electron scattering, which greatly increases the mobilities of charge carriers[12] and greatly reduces the theoretically estimated plasmonic losses.[32] For a plasmon frequency ω_q below the interband Landau-damping threshold, $2E_F/\hbar$, where E_F is the Fermi energy of graphene, and below the optical phonon frequency, $\hbar\omega_o \approx 0.2$ eV, the plasmon relaxation time can be estimated from direct-current measurements. In unsuspended graphene, the high static carrier mobility of $\mu \approx 2.5 \times 10^4$ cm^2 V^{-1} s^{-1} [13,33] is realized at a carrier density of $n \approx 5 \times 10^{12}$ cm^{-2}, which corresponds to $E_F = \hbar v_F \sqrt{\pi n} \approx 0.3$ eV, where $v_F \approx 1.15 \times 10^8$ cm s^{-1} is the Fermi velocity.[35] For this mobility, the plasmon relaxation time in graphene can be

[1]Department of Physics and Astronomy, Georgia State University, Atlanta, GA 30303, USA; [2]Faculty of Physics, Ludwig Maximilian University, D-80539 Munich, Germany and [3]Max Plank Institute for Quantum Optics, D-85748 Garching, Germany
Correspondence: Professor V Apalkov and Professor MI Stockman, Department of Physics and Astronomy, Georgia State University, Atlanta, GA 30303, USA
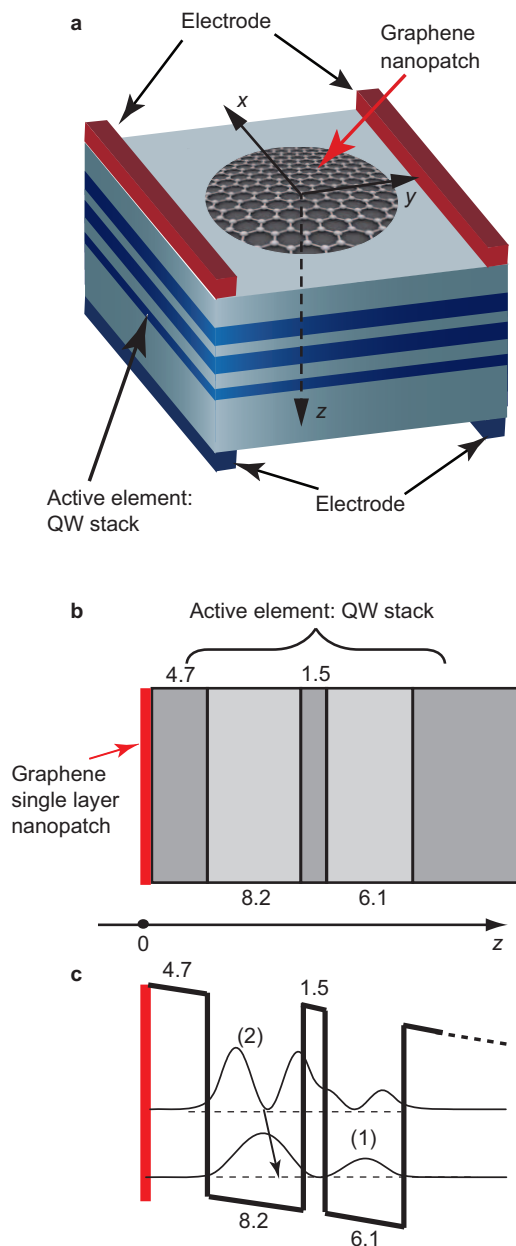E-mail: vapalkov@gsu.edu; mstockman@gsu.edu

Figure 1 Schematic of a graphene quantum cascade nanospaser. (**a**) Geometry of the spaser: monolayer graphene nanopatch on top of a stack of quantum-cascade wells and electrodes for electric pumping (the graphene may be used as one of the electrodes). (**b**) Schematic of the cross-section geometry of the quantum cascade nanospaser. The numbers (in nm) are the widths of the wells ($Ga_{0.47}In_{0.53}As$) and of the barriers ($Al_{0.48}In_{0.52}As$). These wells and barriers are shown in light and dark gray, respectively. (**c**) Energy-band diagram of the active region of a quantum cascade laser structure under an electric field bias. Relative wave functions of sub-bands (1) and (2) as well as the optical transition corresponding to the spaser action are shown schematically.

estimated as $\tau = \mu \hbar \sqrt{\pi n}/(e v_F) \approx 0.6$ ps, which yields a plasmon quality factor of $Q = \omega_q \tau/2 \approx 50$ at a frequency of $\hbar \omega_q = 130$ meV.

As the active element of the graphene spaser, we consider a multi-quantum well system, which is similar to the design of the active element of quantum cascade lasers.[28,36,37] Within the active region of such a multiquantum well structure, optical transitions occur between sub-band levels of dimensional quantization in the growth direction.
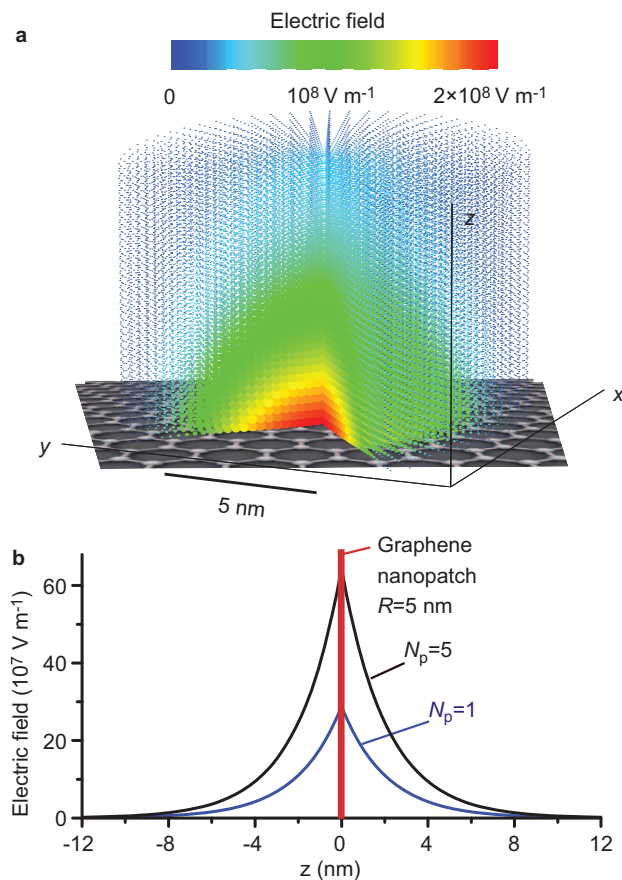

Figure 2 Optical electric field distribution in a graphene nanospaser. (**a**) Spatial distribution of the local optical electric field generated in a spaser with a single surface plasmon in the ground mode on a circular graphene nanopatch with a radius of $R=5$ nm. The three-dimensional distribution (shown over the graphene nanodisk only) is displayed as a 'field cloud', where the field is depicted by points whose color and size correspond to the local amplitude. The spatial scale and the field color-coded scale for the field are indicated. One quarter of the distribution is removed to better display the inner structure of the field. A schematic of the graphene nanopatch is also shown at the bottom. (**b**) The vertical (normal to graphene nanopatch surface) amplitude of the electric field is plotted as a function of z at the center of the graphene nanodisk for two values of the plasmon population, $N_p=1$ and $N_p=5$ as indicated.

In the graphene spaser, we utilize only one period (a single multiquantum well heterostructure) from the vertical-transition active medium of the quantum cascade laser[28] (see Figure 1, in which a possible nanospaser design is illustrated). The functioning of such an active medium is characterized by the electrical injection of electrons into the upper sub-band level of the multiquantum well system and their extraction from the lower sub-band level (Figure 1c). Because the plasmonic modes of graphene are strongly localized in the normal direction (i.e., in the growth direction of the quantum wells, along the z axis in Figure 1), with a localization length of about 3–5 nm, only one period of the quantum cascade gain medium sufficiently couples to the plasmonic modes of graphene. The gain, i.e., population inversion, in the quantum well system is introduced through a voltage applied to the system.

To analytically determine the plasmonic modes of graphene, we assume that the graphene monolayer is surrounded by two homogeneous media with dielectric constants ε_1 and ε_2 (cf. the schematic in Figure 1). Effectively, this approximation corresponds to the replacement of the

cascade system with a homogeneous effective medium. We assume that the graphene monolayer is positioned in the plane $z=0$. Its plasmon wave function (electric field) in the upper half of the plane ($z>0$) is $\propto e^{iqy}e^{-k_{1z}z}$, and its plasmon wave function in the lower half of the plane ($z<0$) is $\propto e^{iqy}e^{-k_{2z}z}$, where q is the in-plane wave vector and k_{1z} and k_{2z} are the decay constants in the upper and lower half planes, respectively.

The spatial distribution of the electric field of plasmonic excitations in graphene and their dispersion relation are determined by solving the Maxwell equations. The corresponding boundary conditions are introduced in terms of a two-dimensional current generated in the graphene layer, which is proportional to the in-plane electric field and is determined by the in-plane conductance, $\sigma(\omega)$, of the graphene. We consider a transverse magnetic plasmon mode in the graphene monolayer that propagates in the y direction with wave vector q, frequency ω_q, and amplitude $\mathcal{E}_q$, where the distribution of the electric field has the following form:[33]

$$E_q = \begin{pmatrix} E_{qz} \\ E_{qy} \end{pmatrix} = \mathcal{E}_q \begin{pmatrix} -i\dfrac{q}{k_{2z}}e^{iqy}e^{k_{2z}z} \\ e^{iqy}e^{k_{2z}z} \end{pmatrix}, \; z<0 \qquad (1)$$

$$E_q = \begin{pmatrix} E_{qz} \\ E_{qy} \end{pmatrix} = \mathcal{E}_q \begin{pmatrix} i\dfrac{q}{k_{1z}}e^{iqy}e^{-k_{1z}z} \\ e^{iqy}e^{-k_{1z}z} \end{pmatrix}, \; z>0 \qquad (2)$$

The corresponding profile of the magnetic field is

$$H_{qx} = \mathcal{E}_q \begin{cases} \dfrac{i\omega_q\varepsilon_1}{ck_{1z}}e^{iqy}e^{-k_{1z}z}, \; z>0 \\[2ex] -\dfrac{i\omega_q\varepsilon_2}{ck_{2z}}e^{iqy}e^{k_{2z}z}, \; z<0 \end{cases} \qquad (3)$$

where c is the speed of light in a vacuum.

The spatial decay of the electromagnetic field away from the graphene layer is determined by the decay rates ('imaginary wave vectors') k_{1z} and k_{2z}, which are given by the following expressions:

$$k_{1z}^2 = q^2 - \varepsilon_1\frac{\omega_q^2}{c^2} \qquad (4)$$

$$k_{2z}^2 = q^2 - \varepsilon_2\frac{\omega_q^2}{c^2} \qquad (5)$$

As justified by the dispersion relation for the surface plasmons in graphene that will be obtained below, for the realistic frequencies under consideration, the plasmon wavelength is much smaller than that of light in a vacuum, i.e., $q \gg \omega/c$. Then, from the Maxwell boundary conditions, we obtain a general dispersion relation for graphene as

$$-q\varepsilon_q(\omega_q) = \varepsilon_1 + \varepsilon_2 \qquad (6)$$

where ε_q is the two-dimensional permittivity of graphene and is defined as $\varepsilon_q = 4\pi d/(S_0 F)$, where F and d are the in-plane electric field and the dipole moment of the graphene sheet induced by this field, respectively, and S_0 is the area of this sheet.

In the Drude approximation,

$$\varepsilon_q(\omega_q) = -\frac{4e_0^2 E_F}{\hbar^2\omega_q(\omega_q+i\gamma)} \qquad (7)$$

where e_0 is the electron charge, E_F is the Fermi energy of electrons in graphene, $\omega < 2E_F$ and γ is the electron polarization relaxation rate, which determines the plasmon dephasing time $\tau = 1/\gamma$. In this approximation,

by substituting Equation (7) into Equation (6), we reproduce the well-known dispersion relation for plasmons in graphene:

$$q(\omega) \approx k_{1z} \approx k_{2z} \approx \frac{\hbar^2(\varepsilon_1+\varepsilon_2)}{4e_0^2 E_F}\omega_q(\omega_q+i\gamma) \qquad (8)$$

To quantize the graphene plasmons, we generalize the previously developed procedure.[1,3] We introduce their electric field operator in the second quantization form,

$$\hat{E} = \sum_q E_q\left(\hat{a}_q^+ + \hat{a}_q\right) \qquad (9)$$

where $\hat{a}_q$ and $\hat{a}_q^+$ are operators of creation and annihilation of a plasmon with wave vector q. The unknown amplitude E_q of the plasmonic mode is determined from the Brillouin expression for the field mean energy in a dispersive medium,[38]

$$\frac{1}{8\pi}\left[\int \mathrm{d}^3 r\frac{\mathrm{d}\omega\varepsilon(\omega,r)}{\mathrm{d}\omega}|E_q(r)|^2 + \int \mathrm{d}^3 r H_{qx}^2(r)\right] = \hbar\omega_q \qquad (10)$$

which yields

$$\mathcal{E}_q = \sqrt{\frac{4\pi\hbar\omega_q q}{S_0(\varepsilon_1+\varepsilon_2)\left(3 - \dfrac{\omega_q}{q}\dfrac{\mathrm{d}q}{\mathrm{d}\omega_q}\right)}} \qquad (11)$$

where S_0 is the area of the graphene sheet patch. For the Drude model of graphene conductance, the plasmon dispersion relation is given by Equation (8). Then, Equation (11) simplifies to

$$\mathcal{E}_q = \sqrt{\frac{4\pi\hbar\omega_q q}{S_0(\varepsilon_1+\varepsilon_2)}} \qquad (12)$$

In the quantum description of the graphene spaser, we introduce the Hamiltonian of the spaser in the form

$$H = \sum_{i=1,2}\sum_k E_i(k)\hat{c}_{i,k}^+\hat{c}_{i,k} + \hbar\sum_q \omega_q\hat{a}_q^+\hat{a}_q \\ + \hbar\sum_{q,k}\Omega_{12}(k,q)\left(\hat{a}_q^+\hat{c}_{1,k}^+\hat{c}_{2,k} + hc\right) \qquad (13)$$

where the first summation describes the Hamiltonian of the gain medium, which consists of two sub-bands $i=1$ and $i=2$ (Figure 1) with energies $E_1(k)=\varepsilon_1+\hbar^2 k^2/2m^*$ and $E_2(k)=\varepsilon_2+\hbar^2 k^2/2m^*$, respectively, $\varepsilon_1 < \varepsilon_2$. Here, m^* is the effective mass of an electron and k is a two-dimensional electron wave vector. The second summation in Equation (13) is the Hamiltonian of plasmons in the graphene layer, where $\hat{a}_q$ and $\hat{a}_q^+$ are operators of annihilation and creation of a plasmon with wave vector q (see Equation (9) above). The last summation is the interaction Hamiltonian, $-\hat{E}\hat{d}$, of plasmonic field $\hat{E}$ with dipole $\hat{d}$ of the gain medium.

The dipole interaction strength in Equation (13) is determined by the corresponding Rabi frequency Ω_{12},

$$\Omega_{12}(k,q) = e_0\mathcal{E}_q\int \mathrm{d}r\psi_{1k}^*(r)E_{qz}z\psi_{2k}(r) \qquad (14)$$

where e_0 is the unit charge, and we have taken into account that for intersubband transitions, the dipole matrix element has only the z component, and ψ_{1k} and ψ_{2k} are electron wave functions with wave vector k of sub-bands 1 and 2, respectively.

Quantization of the graphene surface plasmons yields modes (see Equations (1), (2), (11) and (12) above) that possess extremely tight

nanoconfinement at the graphene nanopatch surface, as illustrated in Figure 2. These local fields form a hot spot indicated in red in Figure 2a, which is only a few nanometers in each of the three dimensions. These fields are coherent, and their amplitude in this hot spot is high, $\mathcal{E} \approx 100$ MV m^{-1} for one plasmon per mode; the field amplitude increases with the number of plasmons as $\mathcal{E} \propto N_P^{1/2}$. The unprecedented field localization characteristic of graphene and the high field amplitude inherent in nanospasers bear potential for various important applications, ranging from nanospectroscopy and sensing to nanolithography.

Assuming for simplicity that electron dynamics in the x, y and z directions are separable, we can factorize the wave functions,

$$\psi_{i\mathbf{k}}(\mathbf{r}) = S_0^{-1/2} \chi_i(z) \exp(i\mathbf{k}\mathbf{r}_\perp) \qquad (15)$$

where $\mathbf{r}_\perp = (x,y)$ is a two-dimensional radius. Then, Equation (14) becomes

$$\Omega_{12}(\mathbf{k},\mathbf{q}) = e_0 \mathcal{E}_q \int dz \chi_1^*(z) e^{-k_{z}z} z \chi_2(z) = \mathcal{E}_q d_{12} e^{-qL} \qquad (16)$$

where $d_{12} \approx e_0 \int dz \chi_1^*(z) z \chi_2(z)$ is the intersubband envelope dipole matrix element and L is a characteristic distance between the graphene monolayer and the active quantum well of the cascade structure.

Introducing the density matrix of the active quantum well of the gain medium, $\rho_{\mathbf{k}}(t)$, we describe the dynamics of the spaser within the density matrix approach, writing the equation for the density matrix as $i\hbar\dot{\rho}_{\mathbf{k}}(t) = [\rho_{\mathbf{k}}(t), H]$. For the stationary regime, we obtain the condition of spasing in the form[1,3]

$$\frac{(\Gamma_{12}+\gamma)^2}{(\omega_{12}-\omega_q)^2 + (\Gamma_{12}+\gamma)^2} \sum_k |\Omega_{12}(\mathbf{k},\mathbf{q})|^2 \geq \gamma \Gamma_{12} \qquad (17)$$

where Γ_{12} is the intersubband polarization-relaxation rate and $\omega_{12} = (\varepsilon_2 - \varepsilon_1)/\hbar$ is the intersubband transition frequency. From this and Equation (16), substituting E_q from Equation (12), we obtain

$$\frac{(\Gamma_{12}+\gamma)^2}{(\omega_{12}-\omega_q)^2 + (\Gamma_{12}+\gamma)^2} \frac{\hbar\omega_q q k_0^2}{(\varepsilon_1+\varepsilon_2)} |d_{12}|^2 e^{-2qL} \geq \gamma \Gamma_{12} \qquad (18)$$

Here, wave vector k_0 is an effective Fermi wave vector, i.e., the largest wave vector of the states, which are partially occupied by electrons in the gain region. Note that only such states contribute to the summation in Equation (17).

At the resonance, i.e., at $\omega_{12} = \omega_q$, the condition of spasing simplifies to

$$\frac{\hbar\omega_q q k_0^2}{\varepsilon_1+\varepsilon_2} |d_{12}|^2 e^{-2qL} \geq \gamma \Gamma_{12} \qquad (19)$$

For given active region parameters, Equation (19) introduces a constraint on the plasmon polarization-relaxation rate γ.

RESULTS AND DISCUSSION

Consider the realistic parameters of the active region (corresponding, e.g., to the structure shown in Figure 1b): $\hbar\omega_{12} = 160$ meV, $d_{12} = 2.5e_0$ nm, and $L \approx 6.5$ nm. Note that here L has been calculated as an effective distance from Equation (16) with envelope wave functions for quantum wells in Figure 1c.

For quantum wells, there is inhomogeneous broadening of intersubband transitions, mainly due to fluctuations in the well thickness and interface roughness,[39] and $\Gamma_{12} \approx 3.6$ meV for a well of our type,

which corresponds to a dephasing time of ~ 18 ps. However, the graphene patch is so small (~ 10 nm in our case) that it is likely to completely lie within one homogeneous domain of the quantum well walls, which is approximately 10–30 nm.[40–42] Consequently, the polarization relaxation rate is expected to be $\Gamma_{12} = \hbar/\tau_{12}$, where τ_{12} is the lifetime for the intersubband transition $|2> \rightarrow |1>$, whose typical value for the quantum well cascade systems is[43,44] $\tau_{12} = \hbar/\Gamma_{12} \approx 1$ ps, corresponding to $\Gamma_{12} \approx 0.66$ meV. We adopt this value for our calculations presented below.

Under the resonant condition, the intersubband transition frequency $\hbar\omega_{12} = 160$ meV, which is equal to the plasmon frequency, corresponds to the plasmon wave vector $q \approx 0.2$ nm^{-1} (Equation (8)). Realistically assuming that $k_0 \approx 0.1$ nm^{-1} and $\varepsilon_1 + \varepsilon_2 \approx 12$, we obtain

$$\gamma \leq 3 \times 10^{-2} \text{eV} \qquad (20)$$

the corresponding plasmon polarization-relaxation time is $\tau \geq 2.2$ fs.

Substituting relation (8) into inequality (19), we obtain a spasing condition as a limitation on τ as

$$\tau \geq \tau_{min} = \frac{4e_0^2 \Gamma_{12} E_F}{\hbar^2 \omega_q^3 k_0^2 |d_{12}|^2} e^{2qL} \qquad (21)$$

The dependence of the minimum plasmon relaxation time, τ_{min}, on the plasmon frequency ω_q is shown in Figure 3a for different Fermi energies E_F of electrons in graphene. The data clearly show that there is a broad range of plasmon frequencies in the mid-infrared $\hbar\omega_q \approx 0.1$–0.3 eV where the required minimum relaxation time is relatively short, $\tau_{min} \approx 10$ fs, so the spasing threshold condition (21) can realistically be satisfied. Outside this range, the minimum relaxation time greatly increases. Fortuitously, typical values of frequencies of intersubband
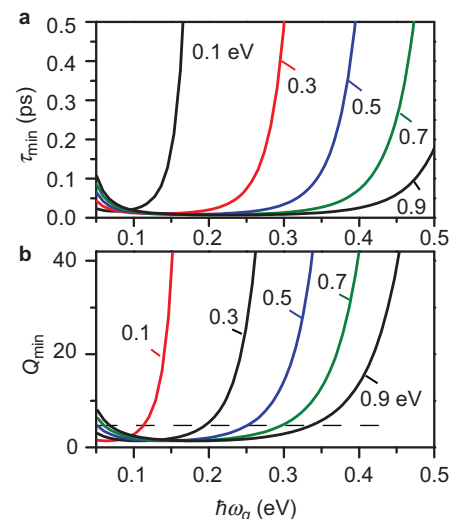

Figure 3 (**a**) Minimum relaxation times of plasmons in graphene sufficient for spasing, as defined by Equation (21), are shown as a function of plasmon frequency for different Fermi energies of electrons in graphene. Spasing occurs for plasmon relaxation times of $\tau > \tau_{min}$. (**b**) The minimum plasmon quality factor Q_{min}, which is sufficient for spasing, as defined by Equation (22), is shown as a function of the plasmon frequency ω_q. The dashed line shows the experimental value of the plasmon quality factor $Q \approx 4$.[27] The numbers next to the lines in (**a**) and (**b**) are the Fermi energies in eV. The results are shown for $L = 6.5$ nm and $d_{12} = 2.5e_0$ nm.

transitions in quantum wells are within the same mid-infrared range of 0.1–0.3 eV.

The spasing condition of Equation (21) can also be expressed in terms of a dimensionless parameter—the plasmon quality factor $Q=\omega_q\tau/2=\omega_q/(2\gamma)$

$$Q \gtrsim Q_{min} \qquad (22)$$

Condition (22) on the surface plasmon quality factor depends on the plasmon frequency, ω_q, which, under resonant conditions, is equal to the frequency of intersubband optical transitions in the active region of the cascade system. As a function of frequency ω_q, the minimum sufficient quality factor, Q_{min}, has a deep minimum, the position of which is determined by the condition $q\approx 1/2L$ or $\omega_q \approx \{2e_0^2 E_F/[L\hbar^2(\varepsilon_1+\varepsilon_2)]\}^{1/2}$, and it depends on the parameters of the system, such as the Fermi energy of the electrons in graphene, E_F, and the effective distance, L, between the graphene monolayer and the active quantum well of the cascade structure. The dependence of Q_{min} on the frequency of surface plasmons, ω_q is shown in Figure 3b for different Fermi energy E_F values. The minimum value of Q is $Q_{min}=2eL\Gamma_{12}(\varepsilon_1+\varepsilon_2)/(k_0^2|d_{12}|^2)\approx 1.5$ and it does not depend on the Fermi energy, which only affects the position of this minimum. This minimum required quality factor of the plasmons is in fact very low, which implies that the spasing is relatively easy to achieve. In fact, the quality factor value $Q\approx 50$, which is obtained for graphene from the experimental data discussed in the 'Introduction Section', is high enough, $Q>>Q_{min}$ (it is on the same order as that for silver in the visible region[18]), for spasing to occur over a broad range of frequencies ω_q (Figure 3b).

The plasmon damping rate in graphene was directly measured using mid-infrared nanoscopy.[27] The best fit to the experimental data was obtained for rather strong damping or a low quality factor, $Q\approx 4$, at a plasmon frequency of $\hbar\omega_q=0.11$ eV, which corresponds to a plasmon relaxation time of $\tau=44$ fs. Even for such strong plasmon damping, the plasmon quality factor, $Q\approx 4$, is greater than the minimum required value rate, $Q_{min}\approx 1.5$ (Figure 3b). Considering that the plasmon relaxation rate strongly increases above the optical phonon frequency, $\hbar\omega_0\approx 0.2$ eV, we can conclude that the optimal Fermi energy in graphene should be $E_F\approx 0.15$ eV. For this Fermi energy, the minimum of Q_{min} is realized at the plasmon frequency in the mid-infrared, $\hbar\omega_q\approx 0.15$ eV (Figure 3b). The above results clearly suggest that spasing can be achieved in realistic graphene systems coupled to quantum cascade well structures.

Note that if the inhomogeneous width of the quantum-well intersubband transition, $\Gamma_{12}=3.6$ meV, were used rather than the much smaller homogeneous width, $\Gamma_{12}=0.66$ meV, then the required minimum quality factor would increase to $Q_{min}\approx 7.5$. This value also appears to be within a realistic range for graphene to be sufficient for spasing.

CONCLUSION

We predict that a graphene monolayer nanopatch deposited on the top of a specially designed stack of quantum wells constitutes an electrically pumped spaser, which is a coherent source of surface plasmons and intense local optical fields in graphene in the mid-infrared. The system of quantum wells is designed similar to the active element of a quantum cascade laser and is characterized by an efficient electrical injection of electrons into an upper sub-band level of the multi-quantum well system and rapid extraction of electrons from a lower sub-band level.

The proposed graphene spaser consists of two main elements. The first element is a graphene nanopatch, which supports the surface plasmon excitations with an optical field strongly localized near the graphene layer, i.e., in the direction perpendicular to the layer. The second element is an active medium, which is a multi-quantum well system. This system is electrically pumped, which results in an inversion population of the quantum well sub-band levels. The optical transitions between the sub-band levels are coupled to plasmon excitations through the optical field. Thus, the transitions in the active medium between the sub-band levels generate the coherent surface plasmons in the graphene nanopatch. The frequency of interband optical transitions in the gain medium (multiquantum well system) determines the frequency of the surface plasmons generated in the graphene layer. For a graphene spaser with a large-size graphene patch, i.e., with the 2D graphene layer, the generated surface plasmons, the frequency of which is equal to the frequency of intersubband optical transitions in the multiquantum system, are characterized by the corresponding wave vector, q. This wave vector also determines the smallest size of the graphene nanopatch $R\approx 1/q$ that can be used in the graphene spaser and that supports the plasmon modes with a frequency equal to the frequency of the intersubband optical transitions in the active medium. In this case, the size of the graphene nanopatch should be adjusted so that it supports the corresponding plasmon modes. Thus, in a graphene spaser, both a large-size graphene patch and a small graphene nanopatch can be used. For the large-size patch, which has a quasi-continuous plasmon spectrum, the frequency of the generated plasmons is automatically selected by the gain medium, whereas for the graphene nanopatch, the geometry of the nanopatch should support the plasmons with a frequency corresponding to the frequency of the active medium.

For realistic parameters of the multiple quantum wells, our analysis shows that the condition of spasing, i.e., coherent generation of plasmons in graphene, can be achieved under realistic conditions with finite doping of the graphene monolayer corresponding to a Fermi energy of electrons in graphene of $E_F\approx 0.15$ eV. The above analysis can be applied not only to a graphene monolayer, but also to graphene-based nanoscale structures such as graphene nanoribbons, graphene quantum dots, and graphene nanoantennas, in particular nanodimers, where the possibility of efficient nanofocusing has recently been proposed.[17] The predicted graphene spaser will be an efficient source of intense and coherent nanolocalized fields in the mid-infrared spectrum (cf. Figure 2). Because the size of such a near-field localized mid-infrared source ≤ 10 nm is on the same order of magnitude as important biological objects (viruses, cell organelles, chromosomes, large proteins, or DNA) and technological elements (transistors and interconnects), such a spaser, will have potential widespread applications in fields such as mid-infrared nanoscopy, nanospectroscopy, nanolithography, biomedicine and nano-optoelectronics.

1   Bergman DJ, Stockman MI. Surface plasmon amplification by stimulated emission of radiation: quantum generation of coherent surface plasmons in nanosystems. *Phys Rev Lett* 2003; **90**: 027402.

2   Stockman MI. Spasers explained. *Nat Photonics* 2008; **2**: 327–329.

3   Stockman MI. The spaser as a nanoscale quantum generator and ultrafast amplifier. *J Opt* 2010; **12**: 024004.

4   Noginov MA, Zhu G, Belgrave AM, Bakker R, Shalaev VM *et al*. Demonstration of a spaser-based nanolaser. *Nature* 2009; **460**: 1110–1112.

5   Hill MT, Marell M, Leong ES, Smalbrugge B, Zhu Y *et al*. Lasing in metal-insulator-metal subwavelength plasmonic waveguides. *Opt Express* 2009; **17**: 11107–11112.

6   Oulton RF, Sorger VJ, Zentgraf T, Ma RM, Gladden C *et al*. Plasmon lasers at deep subwavelength scale. *Nature* 2009; **461**: 629–632.

7   Ma RM, Oulton RF, Sorger VJ, Bartal G, Zhang X. Room-temperature sub-diffraction-limited plasmon laser by total internal reflection. *Nat Mater* 2010; **10**: 110–113.

8   Flynn RA, Kim CS, Vurgaftman I, Kim M, Meyer JR *et al*. A room-temperature semiconductor spaser operating near 1.5 micron. *Opt Express* 2011; **19**: 8954–8961.

9   van Beijnum F, van Veldhoven PJ, Geluk EJ, de Dood MJ, 't Hooft GW *et al*. Surface plasmon lasing observed in metal hole arrays. *Phys Rev Lett* 2013; **110**: 206802.

10 Zhou W, Dridi M, Suh JY, Kim CH, Co DT *et al*. Lasing action in strongly coupled plasmonic nanocavity arrays. *Nat Nanotechnol* 2013; **8**: 506–511.

11 Lu YJ, Kim J, Chen HY, Wu C, Dabidian N *et al*. Plasmonic nanolaser using epitaxially grown silver film. *Science* 2012; **337**: 450–453.

12 Novoselov KS, Geim AK, Morozov SV, Jiang D, Katsnelson MI *et al*. Two-dimensional gas of massless dirac fermions in graphene. *Nature* 2005; **438**: 197–200.

13 Zhang YB, Tan YW, Stormer HL, Kim P. Experimental observation of the quantum hall effect and berry's phase in graphene. *Nature* 2005; **438**: 201–204.

14 Sirtori C, Faist J, Capasso F, Sivco DL, Hutchinson AL *et al*. Quantum cascade laser with plasmon-enhanced wave-guide operating at 8.4 μm wavelength. *Appl Phys Lett* 1995; **66**: 3242–3244.

15 Tredicucci A, Gmachl C, Capasso F, Hutchinson AL, Sivco DL *et al*. Single-mode surface-plasmon laser. *Appl Phys Lett* 2000; **76**: 2164–2166.

16 Walther C, Scalari G, Amanti MI, Beck M, Faist J. Microcavity laser oscillating in a circuit-based resonator. *Science* 2010; **327**: 1495–1497.

17 Thongrattanasiri S, de Abajo FJ. Optical field enhancement by strong plasmon interaction in graphene nanostructures. *Phys Rev Lett* 2013; **110**: 187401.

18 Stockman MI. Nanoplasmonics: past, present, and glimpse into future. *Opt Express* 2011; **19**: 22029–22106.

19 Heeres RW, Kouwenhoven LP, Zwiller V. Quantum interference in plasmonic circuits. *Nat Nanotechnol* 2013; **8**: 719–722.

20 Moskovits M. Surface-enhanced spectroscopy. *Rev Mod Phys* 1985; **57**: 783–826.

21 Kneipp J, Kneipp H, Wittig B, Kneipp K. Novel optical nanosensors for probing and imaging live cells. *Nanomed Nanotechnol Biol Med* 2010; **6**: 214–226.

22 Xu HX, Bjerneld EJ, Kall M, Borjesson L. Spectroscopy of single hemoglobin molecules by surface enhanced Raman scattering. *Phys Rev Lett* 1999; **83**: 4357–4360.

23 Tang L, Kocabas SE, Latif S, Okyay AK, Ly-Gagnon DS *et al*. Nanometre-scale germanium photodetector enhanced by a near-infrared dipole antenna. *Nat Photonics* 2008; **2**: 226–229.

24 Nagatani N, Tanaka R, Yuhi T, Endo T, Kerman K *et al*. Gold nanoparticle-based novel enhancement method for the development of highly sensitive immunochromatographic test strips. *Sci Technol Adv Mater* 2006; **7**: 270–275.

25 Cole JR, Mirin NA, Knight MW, Goodrich GP, Halas NJ. Photothermal efficiencies of nanoshells and nanorods for clinical therapeutic applications. *J Phys Chem C* 2009; **113**: 12090–12094.

26 Huber A, Ocelic N, Kazantsev D, Hillenbrand R. Near-field imaging of mid-infrared surface phonon polariton propagation. *Appl Phys Lett* 2005; **87**: 081103.

27 Fei Z, Rodin AS, Andreev GO, Bao W, McLeod AS *et al*. Gate-tuning of graphene plasmons revealed by infrared nano-imaging. *Nature* 2012; **487**: 82–85.

28 Faist J, Capasso F, Sirtori C, Sivco DL, Hutchinson AL *et al*. Vertical transition quantum cascade laser with Bragg confined excited-state. *Appl Phys Lett* 1995; **66**: 538–540.

29 Geim AK, Novoselov KS. The rise of graphene. *Nat Mater* 2007; **6**: 183–191.

30 Neto AH, Guinea F, Peres NM, Novoselov KS, Geim AK. The electronic properties of graphene. *Rev Mod Phys* 2009; **81**: 109–162.

31 Abergel DS, Apalkov V, Berashevich J, Ziegler K, Chakraborty T. Properties of graphene: a theoretical perspective. *Adv Phys* 2010; **59**: 261–482.

32 Koppens FH, Chang DE, de Abajo FJ. Graphene plasmonics: a platform for strong light-matter interactions. *Nano Lett* 2011; **11**: 3370–3377.

33 Jablan M, Buljan H, Soljacic M. Plasmonics in graphene at infrared frequencies. *Phys Rev B* 2009; **80**: 245435.

34 Grigorenko AN, Polini M, Novoselov KS. Graphene plasmonics. *Nat Photonics* 2012; **6**: 749–758.

35 Kim S, Jo I, Dillen DC, Ferrer DA, Fallahazad B *et al*. Direct measurement of the Fermi energy in graphene using a double-layer heterostructure. *Phys Rev Lett* 2012; **108**: 116404–116407.

36 Kazarinov RF, Suris RA. Possibility of amplification of electromagnetic waves in a semiconductor with a superlattice. *Sov Phys Semicond* 1971; **5**: 707.

37 Faist J, Capasso F, Sivco DL, Sirtori C, Hutchinson AL *et al*. Quantum cascade laser. *Science* 1994; **264**: 553–556.

38 Landau LD, Lifshitz EM. *Electrodynamics of Continuous Media*. Oxford/New York: Pergamon; 1984.

39 Campman KL, Schmidt H, Imamoglu A, Gossard AC. Interface roughness and alloy-disorder scattering contributions to intersubband transition linewidths. *Appl Phys Lett* 1996; **69**: 2554–2556.

40 Juang FY, Bhattacharya P, Singh J. Determination of the microscopic quality of InGaAs/InAlAs interfaces by photoluminescence—role of interrupted molecular beam epitaxial growth. *Appl Phys Lett* 1986; **48**: 290–292.

41 Bimberg D, Oertel D, Hull R, Reid G, Carey K. Detailed atomic scale structure of AlInAs/GaInAs quantum wells. *J Appl Phys* 1989; **65**: 2688–2692.

42 Bernatz G, Nau S, Rettig R, Jansch H, Stolz W. Experimental investigation of structures of interior interfaces in GaAs. *J Appl Phys* 1999; **86**: 6752–6757.

43 Ferreira R, Bastard G. Evaluation of some scattering times for electrons in unbiased and biased single- and multiple-quantum-well structures. *Phys Rev B* 1989; **40**: 1074–1086.

44 Yamanishi M, Edamura T, Fujita K, Akikusa N, Kan H. Theory of the intrinsic linewidth of quantum cascade lasers: hidden reason for the narrow linewidth and line-broadening by thermal photons. *IEEE J Quantum Electron* 2008; **44**: 12–29.